Numerical Heat Transfer, Part A, 43: 603–617, 2003

1040-7782/03 $12.00 + .00
DOI: 10.1080/10407780390122989

NUMERICAL ANALYSIS OF THE STRESS JUMP INTERFACE CONDITION FOR LAMINAR FLOW OVER A POROUS LAYER

Renato A. Silva and Marcelo J. S. de Lemos
Departamento de Energia—IEME, Instituto Tecnológico de Aeronáutica—ITA, São Paulo, Brazil.

A number of natural and engineering systems can be characterized by some sort of porous structure through which a working fluid permeates. Boundary layers over tropical forests and spreading of chemical contaminants through underground water reservoirs are examples of important environmental flows that can benefit form appropriate mathematical treatment. For hybrid media, involving both a porous structure and a clear flow region, difficulties arise due to the proper mathematical treatment given at the interface. The literature proposes a jump condition in which stresses at both sides of the interface are not of the same value. The objective of this article is to present a numerical implementation for solving such a hybrid medium, considering here a channel partially filled with a porous layer through which fluid flows in laminar regime. One unique set of transport equations is applied to both regions. Numerical results are compared with available analytical solutions in the literature for two cases, namely, with and without the nonlinear Forchheimer term. Results are presented for the mean velocity across both the porous structure and the clear region. The influence of medium properties, such as porosity and permeability, is discussed.

INTRODUCTION

Recently, there has been growing awareness of the need to preserve the environment. The study of atmospheric boundary-layer flows over rain forests and vegetation could bring insight to scientists about overall exchange rates of mass and energy between the soil and the atmosphere. In this sense, proper mathematical modeling of such flows could be advantageous for more realistic analyses of the environment. Accordingly, environmental flows like those could be characterized by a hybrid domain, consisting of a clear region and a layer of a permeable medium, over which air flows around the interface between the two media.

Traditional modeling of flow in porous medium makes use of macroscopic variables and transport equations [1–5] where volume average properties are obtained by means of proper mathematical tools [6, 7]. For flow presenting a

Received 12 April 2002; accepted 11 July 2002.
The authors are thankful to CAPES and CNPq, Brazil, for their financial support during the course of this research.
Address correspondence to M. J. S de Lemos, Departamento de Energia, IEME—ITA—CTA, 12228-900 São José dos Campos, São Paulo, Brazil. E-mail: delemos@mec.ita.br

NOMENCLATURE

A_i	macroscopic interface area between the porous region and the clear flow	$\mathbf{u}$	microscopic (local) velocity vector
A_i^m	microscopic interfacial area between the solid and the liquid phases	$\langle \mathbf{u} \rangle^i$	intrinsic (fluid) average of $\mathbf{u}$
c_F	Forchheimer coefficient in Eq. (7)	$\mathbf{u}_D$	Darcy velocity vector (volume average over $\mathbf{u}$) $(= \phi \langle \mathbf{u} \rangle^i)$
Da	Darcy number $(= K/H^2)$	$\mathbf{u}_{D_i}$	Darcy velocity vector at the interface
H	distance between the channel walls	$\mathbf{u}_{D_p}$	Darcy velocity vector parallel to the interface
K	permeability	u_{D_n}, u_{D_p}	components of Darcy velocity at interface along η (normal) and ξ (parallel) directions, respectively
l	distance from the lower wall to the center of the porous medium	u_{D_i}, v_{D_i}	components of Darcy velocity at interface along x and y, respectively
L	axial length of periodic section of channel	x, y	Cartesian coordinates
$\mathbf{n}$	unit vector normal to the interface	β	interface stress jump coefficient
$\mathbf{p}$	unit vector parallel to the interface	η, ξ	generalized coordinates
p	thermodynamic pressure	μ	dynamic viscosity
$\langle p \rangle^i$	intrinsic (fluid) average of pressure p	μ_{eff}	effective viscosity for a porous medium
$\mathbf{R}$	total drag per unit volume	ρ	density
Re_H	Reynolds number based on the channel height $(= \rho \lvert \mathbf{u}_D \rvert H/\mu)$	ϕ	porosity
s	clear region thickness	φ	general dependent variable
S_φ	source term		

macroscopic interfacial area, the literature proposes the existence of a stress jump interface condition between the clear flow region and the porous medium [8, 9]. This model for the flow near an interface has been investigated analytically for a channel partially filed with a porous material. Solutions in such composite channels not considering the nonlinear Forchheimer term have been presented [10]. Additional work extending that analytical technique for including nonlinear effects has also been presented [11, 12]. Although exact in nature, such solutions are limited to one-dimensional, fully developed flow and for that reason they are of limited application in simulating real three-dimensional engineering flows.

Purely numerical solutions for two-dimensional hybrid medium (porous region-clear flow) in an isothermal channel has been considered in [13] based on the turbulence model proposed in [14–16]. That work has been developed under the double-decomposition concept [17–19], a new methodology recently compared with other views in the literature [20]. Nonisothermal flow in channels past a porous obstacle [21] and through a porous insert have also been presented [22]. In all previous work [13, 21, 22], the interface boundary condition considered a continuous function for the stress field across the interface.

Recently, numerical solutions not considering the nonlinear term in the macroscopic momentum equation for composite channels have been presented [23]. Also simulated was the case when nonlinear effects were introduced [24]. Such works were based on the numerical methodology proposed for hybrid media and applied in [13, 21, 22].

The objective of this work is to document the numerical methodology followed when implementing the stress jump boundary condition. Such implementation is based on the mathematical treatment given in [8, 9]. For checking the numerical accuracy of the solution, comparisons with analytical distributions are carried out.

Effects of grid size, Reynods number, permeability K, and porosity ϕ variation are investigated.

MACROSCOPIC MODEL

Geometry

The flows investigated here are shown schematically in Figure 1. The channels are partially filled with a layer of a porous material. A constant-property fluid flows longitudinally from left to right, permeating through both the clear region and the porous structure. The case in the Figure 1a uses symmetry boundary condition at the channel center ($y = 0$), whereas in Figure 1b a solid wall in assumed at the bottom

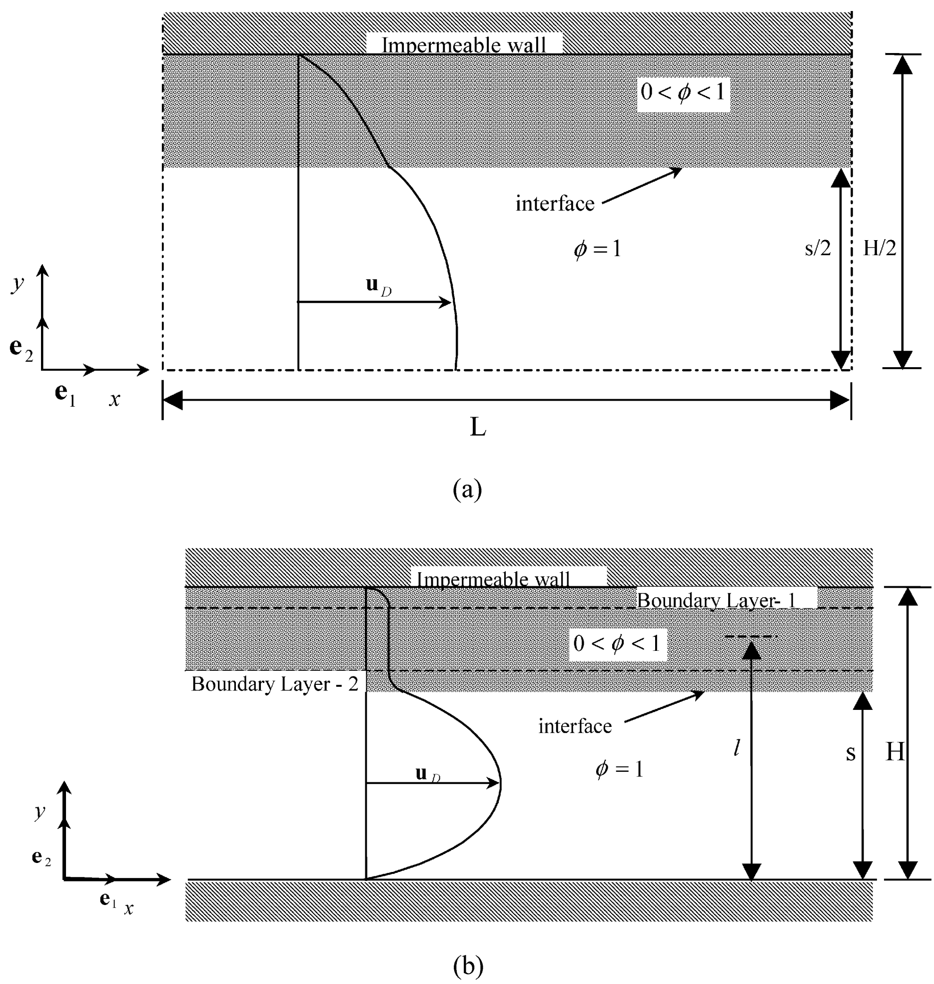

Figure 1. Model for channel flow with porous material: (a) without the Forchheimer term; (b) with the Forcheimer term.

surface. Also, in Figure 1, H is the distance between the channel walls and s is the clearance for the nonobstructed flow passage.

Governing Equations

A macroscopic form of the governing equations is obtained by taking the volumetric average of the entire equation set. In this development, the porous medium is considered to be rigid, undeformable, and saturated by an incompressible fluid.

The microscopic continuity equation for the fluid phase is given by

$$\nabla \cdot \mathbf{u} = 0 \tag{1}$$

Applying the volume-average operator to Eq. (1), one has (see [14])

$$\nabla \cdot \mathbf{u}_D = 0 \tag{2}$$

where the local velocity vector $\mathbf{u}$ is of null value at the local interfacial area A_i^m (not to be confused with the macroscopic interface area A_i) and the Dupuit-Forchheimer relationship, $\mathbf{u}_D = \phi\langle\mathbf{u}\rangle^i$, has been used, where the operator "$\langle\ \rangle$" identifies the intrinsic (liquid volume-based) average of $\mathbf{u}$ [7]. Equation (2) represents the macroscopic continuity equation for an incompressible fluid in a rigid porous medium.

The microscopic Navier–Stokes equation for an incompressible fluid with constant properties can be written as

$$\rho\left[\frac{\partial \mathbf{u}}{\partial t} + \nabla \cdot (\mathbf{u}\mathbf{u})\right] = -\nabla p + \mu\nabla^2\mathbf{u} \tag{3}$$

Hsu and Cheng [5] have applied the volume-averaging procedure to Eq. (3), obtaining

$$\rho\left[\frac{\partial}{\partial t}(\phi\langle\mathbf{u}\rangle^i) + \nabla \cdot (\phi\langle\mathbf{u}\mathbf{u}\rangle^i)\right] = -\nabla(\phi\langle p\rangle^i) + \mu\nabla^2(\phi\langle\mathbf{u}\rangle^i) + \mathbf{R} \tag{4}$$

where

$$\mathbf{R} = \frac{\mu}{\Delta V}\int_{A_i^m} \mathbf{n} \cdot (\nabla\mathbf{u})\, dS - \frac{1}{\Delta V}\int_{A_i^m} \mathbf{n}p\, dS \tag{5}$$

The term $\mathbf{R}$ represents the total drag per unit volume acting on the fluid by the action of the porous structure. A common model for it is known as the Darcy–Forchheimer extended model and is given by

$$\bar{\mathbf{R}} = -\left(\frac{\mu\phi}{K}\mathbf{u}_D + \frac{c_F\phi\rho|\mathbf{u}_D|\mathbf{u}_D}{\sqrt{K}}\right) \tag{6}$$

where the constant c_F is known in the literature as the nonlinear Forchheimer coefficient.

Then, making use again of the expression $\mathbf{u}_D = \phi\langle\mathbf{u}\rangle^i$, Eq. (6) can be rewritten as

$$\rho\left[\frac{\partial \mathbf{u}_D}{\partial t} + \nabla\cdot\left(\frac{\mathbf{u}_D\mathbf{u}_D}{\phi}\right)\right] = -\nabla(\phi\langle p\rangle^i) + \mu\nabla^2\mathbf{u}_D - \left(\frac{\mu\phi}{K}\mathbf{u}_D + \frac{c_F\phi\rho|\mathbf{u}_D|\mathbf{u}_D}{\sqrt{K}}\right) \tag{7}$$

Interface Condition between the Clear Fluid and the Porous Medium

The equation proposed in [8, 9] for describing the stress jump at the interface between the clear flow region and the porous structures is given by

$$\mu_{\text{eff}}\frac{\partial u_{D_\xi}}{\partial \eta}\bigg|_{\text{porous medium}} - \mu\frac{\partial u_{D_\xi}}{\partial \eta}\bigg|_{\text{clear fluid}} = \beta\frac{\mu}{\sqrt{K}}u_{D_\xi}\bigg|_{\text{interface}} \tag{8}$$

where u_{D_ξ} is the Darcy velocity component parallel to the interface aligned with the direction ξ and normal to the direction η, μ_{eff} is the effective viscosity for the porous region, μ is the fluid dynamic viscosity, K is the permeability, and β is an adjustable coefficient which accounts for the stress jump at the interface. Equation (8) will be later adapted to the geometry and coordinate system employed here.

NUMERICAL MODEL

The numerical method used for discretizing the system of equations is the control-volume method of Patankar [25]. In the implementation here, a system of generalized coordinates was used, although all simulation to be shown employed only Cartesian coordinates. Nevertheless, the use of a general system $\eta-\xi$ for discretizing the equations was found to be adequate for future simulations.

Because the entire derivation is set up for solving two-dimensional flows, both cases employ the spatially periodic boundary condition along the coordinate. This is done in order to simulate fully developed flow, for which analytical solutions are available for comparison. The spatially periodic condition is implemented by running the solution repetitively, until outlet profiles in $x = L$ match those at the inlet ($x = 0$). Figure 2*a* shows a general control volume in a two-dimensional configuration. The faces of the volume are formed by lines of constant coordinates η–ξ.

For steady state, a general form of the discrete equations for a general variable φ becomes

$$I_e + I_w + I_n + I_s = S_\varphi \tag{9}$$

where $I_e,\ I_w,\ I_n,$ and I_s are the fluxes of φ at faces *east*, *west*, *north*, and *south* of the control volume of Figure 2*a*, respectively, and S_φ is a source term. Details on the numerical methodology employed in obtaining (9) can be found in [15]. Here, all computations were carried out until the residue of the algebraic equations was brought down to 10^{-7}, where the residue was defined as the difference between the right and left sides of the discretized equations.

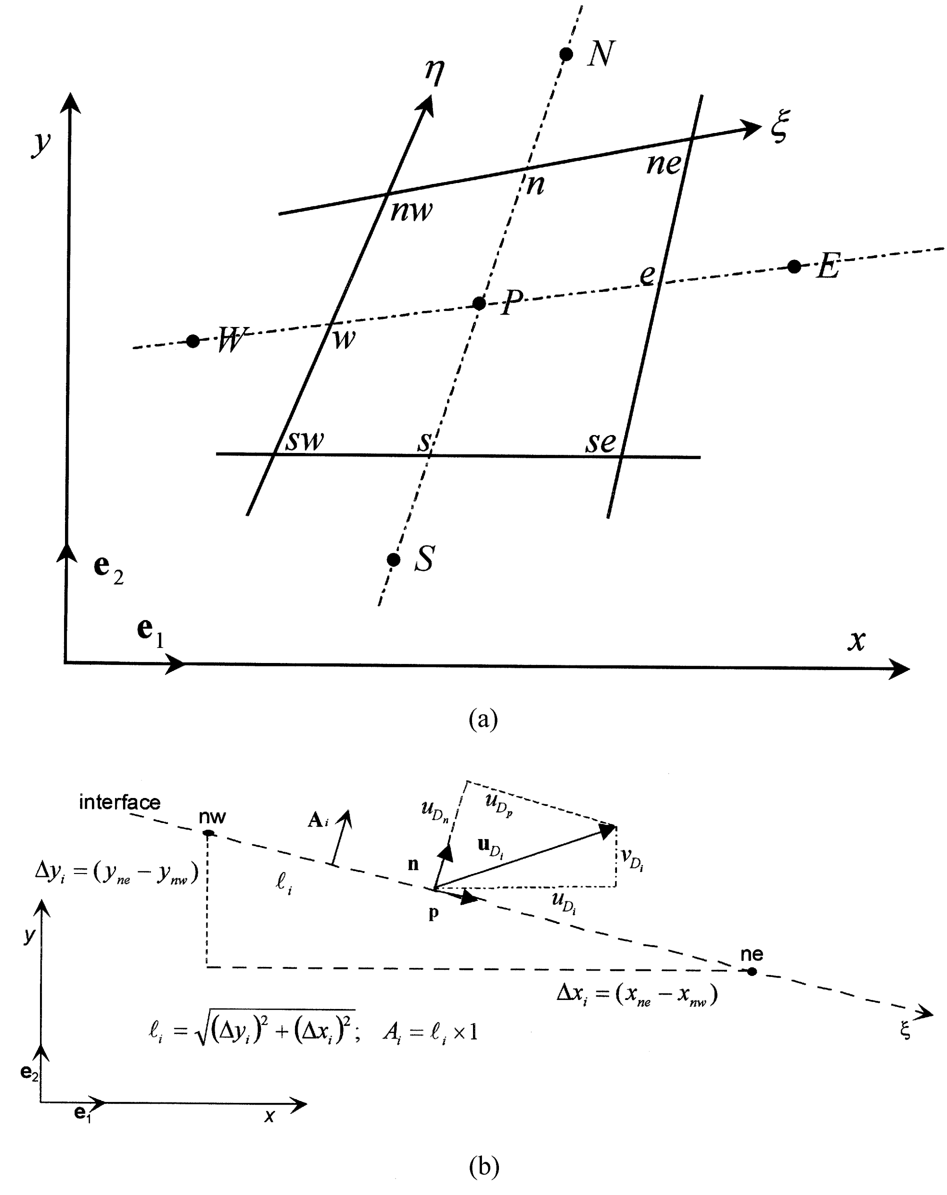

Figure 2. Notation for: (*a*) control volume discretization; (*b*) interface treatment.

Implementation of the Interface Condition

For hybrid domains, in addition to Eq. (8), continuity of velocity and pressure fields prevailing at the interface is given by

$$\mathbf{u}_D|_{0<\phi<1} = \mathbf{u}_D|_{\phi=1} \tag{10}$$

$$\langle p\rangle^i|_{0<\phi<1} = \langle p\rangle^i|_{\phi=1} \tag{11}$$

Conditions (8), (10), and (11) were proposed in [8], using the concept of stress jump at the interface.

Figure 2*b* show details of the interface dividing two control volumes, one being located in the porous region and the other lying in the clear fluid. The computational grid based on generalized coordinate system η–ξ is such that the interface coincides with a line of constant η, extending along the ξ coordinate. In this arrangement, the interface between the two neighbor volumes, each one located at each side of the interface, belongs to both faces of the two volumes. Thus, according to Figure 2*b*, $\mathbf{u}_{D_i}$ is the Darcy velocity at the interface and u_{D_F} its component parallel to the interface itself. It is interesting to point out that although the results presented here are based on an orthogonal Cartesian coordinate system, the derivation to follow is extended to a general system of coordinates η–ξ, the only restriction being the alignment of the interface with a line of constant coordinate. The motivation behind this generalization is to prepare the numerical tool for future use in a complex geometry.

The terms on the left of (8) were discretized according to the nomenclature shown in Figure 2*a*. Details of the derivation can be found in [15] and need not be repeated here. This work focuses on the handling of the term on the right of (8), for which a detailed study is presented below.

Returning to Figure 2*b*, one can identify all variables located at the interface. According to the figure, the Darcy velocity at the interface is given by $\mathbf{u}_{D_i}$. It can be written in either the x–y or η–ξ coordinate system as

$$\mathbf{u}_{D_i} = u_{D_i}\mathbf{e}_1 + v_{D_i}\mathbf{e}_2 = u_{D_n}\mathbf{n} + u_{D_p}\mathbf{p} \tag{12}$$

where u_{D_i} and v_{D_i} are the components of $\mathbf{u}_{D_i}$ in the x and y directions, respectively. Likewise, u_{D_n} and u_{D_p} are the $\mathbf{u}_{D_i}$ components along η and ξ, respectively.

The macroscopic interfacial area vector, normal to the surface, can be expressed as

$$\mathbf{A}_i = \mathbf{n}A_i = -(y_{ne} - y_{nw})\mathbf{e}_1 + (x_{ne} - x_{nw})\mathbf{e}_2 = -\Delta y_i\mathbf{e}_1 + \Delta x_i\mathbf{e}_2 \tag{13}$$

The unit vector normal to the interface, $\mathbf{n}$, is given by

$$\mathbf{n} = \frac{\mathbf{A}_i}{|\mathbf{A}_i|} \tag{14}$$

and therefore its orthogonal unit vector, parallel to the interface, is

$$\mathbf{p} = \left[\frac{(x_{ne} - x_{nw})\mathbf{e}_1 + (y_{ne} - y_{nw})\mathbf{e}_2}{\sqrt{(x_{ne} - x_{nw})^2 + (y_{ne} - y_{nw})^2}}\right] \tag{15}$$

Because the geometry considered has two dimensions, one has $|\mathbf{A}_i| = A_i = \ell_i \times 1$, giving, further,

$$\mathbf{p} = \frac{\Delta x_i \, \mathbf{e}_1 + \Delta y_i \, \mathbf{e}_2}{\ell_i} \tag{16}$$

Therefore, the velocity component parallel to the interface, u_{D_p}, can be calculated as the scalar product of (12) and (15) in the form

$$u_{D_p} = \mathbf{u}_{D_i} \cdot \mathbf{p} \tag{17}$$

$$u_{D_p} = \left[\frac{u_{D_i}(x_{ne} - x_{nw}) + \nu_{D_i}(y_{ne} - y_{nw})}{\sqrt{(x_{ne} - x_{nw})^2 + (y_{ne} - y_{nw})^2}} \right] = \frac{u_{D_i} \, \Delta x_i + \nu_{D_i} \, \Delta y_i}{\ell_i} \tag{18}$$

A Darcy velocity vector parallel to the interface, $\mathbf{u}_{D_p}$, is then given by

$$\mathbf{u}_{D_p} = u_{D_p} \mathbf{p} = \frac{u_{D_i} \, \Delta x_i + \nu_{D_i} \, \Delta y_i}{\ell_i} \left[\frac{\Delta x_i \, \mathbf{e}_1 + \Delta y_i \, \mathbf{e}_2}{\ell_i} \right] \tag{19}$$

Integrating the left-hand side of (8) over the macroscopic interfacial area A_i, and considering further constant velocity $\mathbf{u}_{D_p}$ and constant properties prevailing over the integration area, one has

$$\mathbf{I}_i^{\beta_{x,y}} = \int_{A_i} \mu \frac{\beta}{\sqrt{K}} \mathbf{u}_{D_p} \, dA_i \approx \mu_i \frac{\beta}{\sqrt{K}} \mathbf{u}_{D_p} A_i = \mu_i \frac{\beta}{\sqrt{K}} \mathbf{u}_{D_p} \ell_i \tag{20}$$

Making use of (19), one has, further,

$$\mathbf{I}_i^{\beta_{x,y}} = \mu_i \frac{\beta}{\sqrt{K}} \frac{(u_{D_i} \, \Delta x_i + \nu_{D_i} \, \Delta y_i)}{\ell_i} (\Delta x_i \, \mathbf{e}_1 + \Delta y_i \, \mathbf{e}_2) \tag{21}$$

For numerical solution in a general two-dimensional geometry, the momentum equation components in the x and y are obtained by decomposing (21) such that

$$I_i^{\beta_x} = \mu_i \frac{\beta}{\sqrt{K}} \frac{(u_{D_i} \, \Delta x_i + \nu_{D_i} \, \Delta y_i)}{\ell_i} \Delta x_i \tag{22}$$

and

$$I_i^{\beta_y} = \mu_i \frac{\beta}{\sqrt{K}} \frac{(u_{D_i} \, \Delta x_i + \nu_{D_i} \, \Delta y_i)}{\ell_i} \Delta y_i \tag{23}$$

Terms on the right of (22) and (23) are added to the discretized momentum equation components in the directions x and y, respectively, when the nodal point in question has a face coincident with the interface. For ease of implementation, these additional terms are treated in an explicit form and are added to the right-hand side of (9).

RESULTS AND DISCUSSION

The two cases pictured in Figure 1 are associated with solutions of different forms of Eq. (7). Case (*a*) on the top of the figure is solved without the last term on the right of (7). An analytical solution for this case was first proposed in [10]. On the other hand, case (*b*) in the same figure considers a nonlinear term, also referred to in the literature as a Forchheimer term. Analytical distributions for the velocity field were presented in [11, 12]. In both cases, numerical predictions use analytical profiles for validation of the numerical implementation herein.

Grid-independence studies are shown in Figure 3. The figure shows several nondimensional velocity profiles for $\phi = 0.6$, $K = 4 \times 10^{-7}\,\mathrm{m}^2$, and Darcy number $\mathrm{Da} = 4 \times 10^{-3}$, where $\mathrm{Da} = K/H^2$. The value for the coefficient β is set equal to zero for all solutions presented in the figure. The curves indicate that for more than 40 nodal points in the cross-stream direction, the solution is essentially grid-independent. One should point out that the numerical methodology considered here was focused on two-dimensional flows, so that simulating fully developed situation shown in the figures required the use of nodal points along the axial direction and the employment of the spatially periodic condition mentioned earlier. For all runs studied here, a total of 50 nodes in the axial direction was found to suffice.

Figure 4 show the effect of the permeability K reproduced by both the numerical solution and the one-dimensional theoretical treatment. One can see that the greater the permeability, more flow crosses the porous substratum located in the region $0.5 < y/H < 1$. The agreement between numerical and analytical solution can be noted in the figure.

Figure 5 investigates the effect of the value of ϕ on the behavior of the velocity field. Here also, as expected, the greater the porosity, the higher is the mass flow rate within the permeable layer. On should point out, however, that all solutions presented in Figures 4 and 5 are obtained for a fixed Reynolds number, so that overall mass flow rate through the channel was held constant. The use of the pressure gradient when setting up the nondimensional velocity profiles in the figures may misleadingly indicate an increase in the flow rate in the clear passage, at the channel center, for the cases of increasing K or ϕ. Also to note is that results in Figures 4 and 5 are for $\beta = 0$, indicating that even without considering the numerical implementation of the jump condition, the main object of this investigation, the computer code developed seems to reproduce the exact solution correctly. With these preliminary tests done, further results including the jump at the interface can be better assessed.

Extending the foregoing results, Figure 6 finally compares both the analytical and the numerical solution for β varying from -0.5 to 0.5 for a fixed porosity $\phi = 0.6$ and constant Darcy number $\mathrm{Da} = 4 \times 10^{-3}$. Here also, results seem to indicate the correctness of the numerical implementations for the range of the parameters investigated. Ultimately, results in Figure 6 show the appropriateness of the numerical methodology employed here for considering the stress jump at the interface between a porous medium and a clear region.

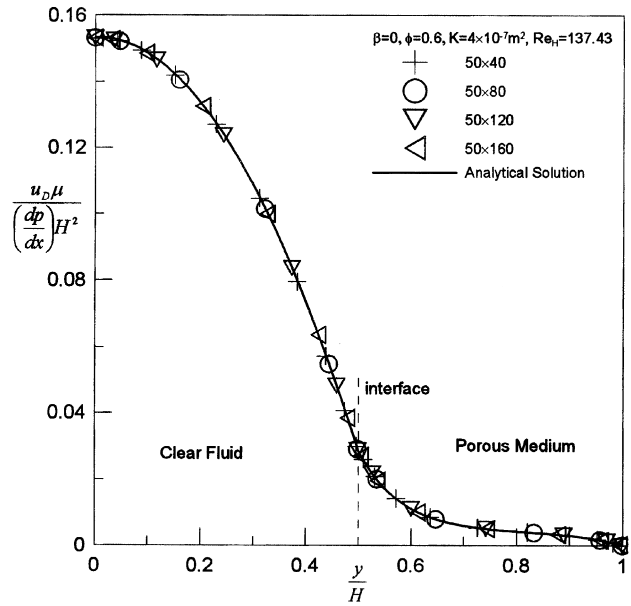

(a)

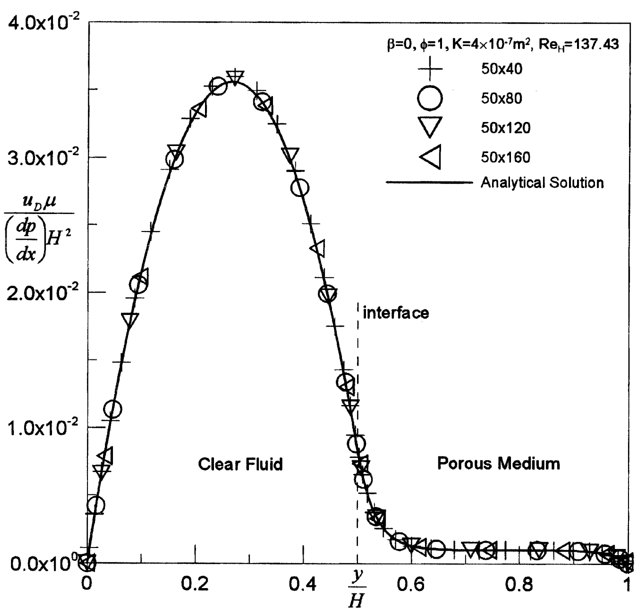

(b)

Figure 3. Effect of grid size on velocity field: (*a*) without the Fochheimer term; (*b*) with the Forchheimer term.

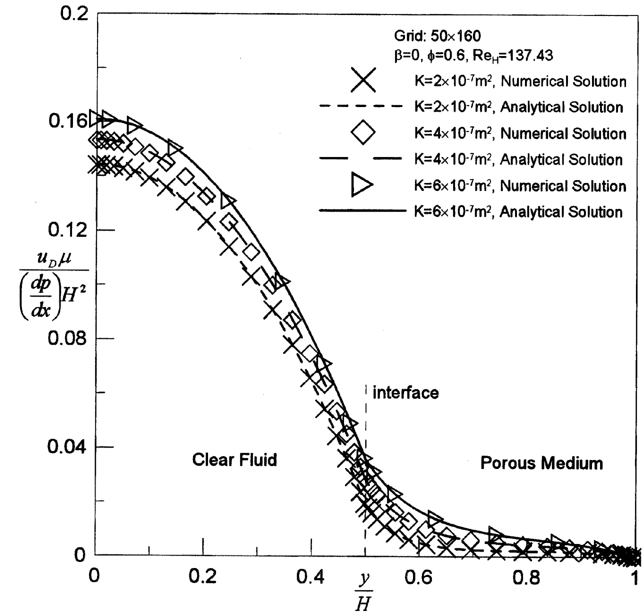

(a)

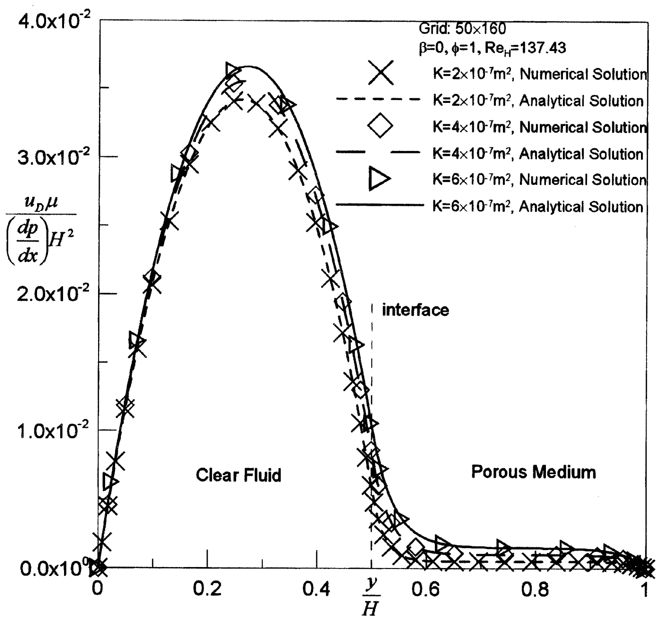

(b)

Figure 4. Comparison between analytical and numerical solution for different permeability, K: (a) without the Fochheimer term; (b) with the Forchheimer term.

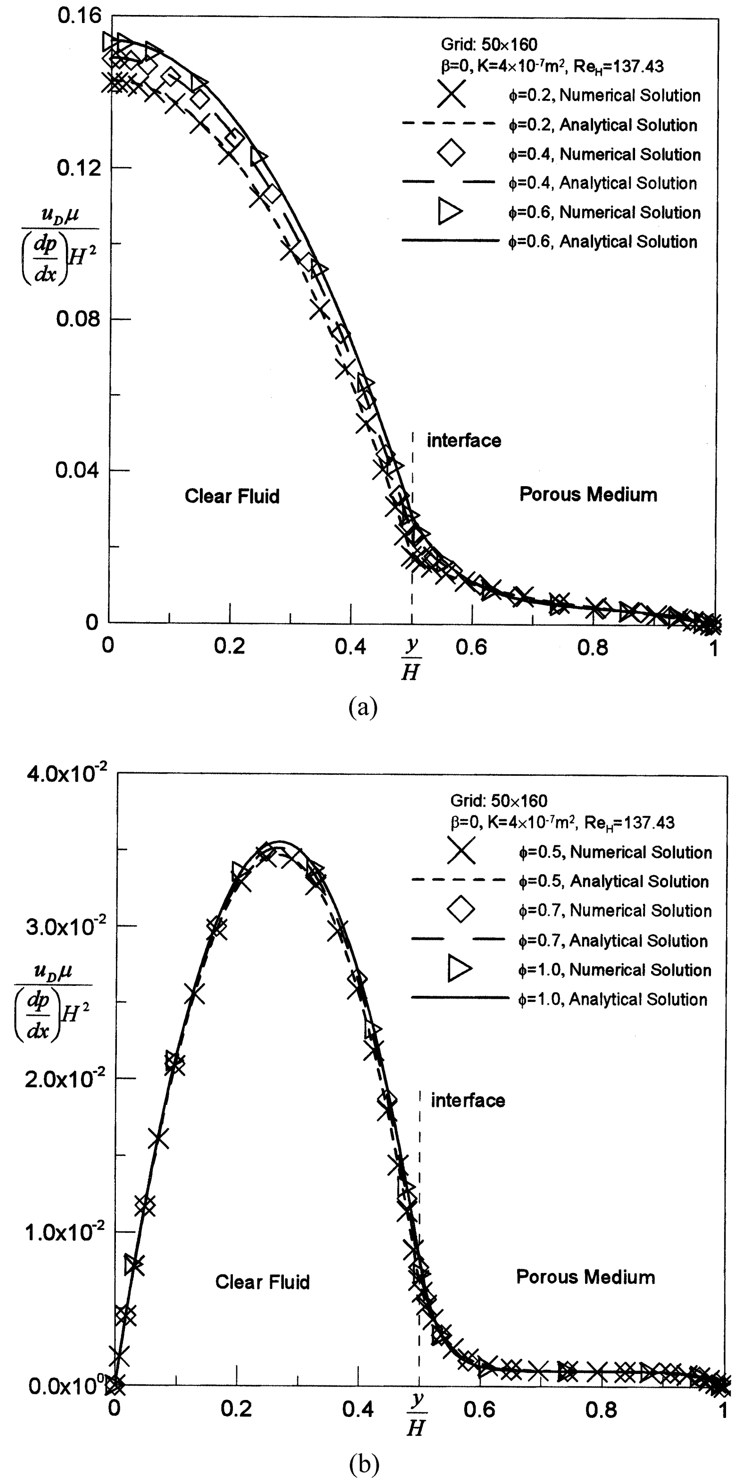

Figure 5. Comparison between analytical and numerical solution for different porosity, ϕ: (*a*) without the Fochheimer term; (*b*) with the Forchheimer term.

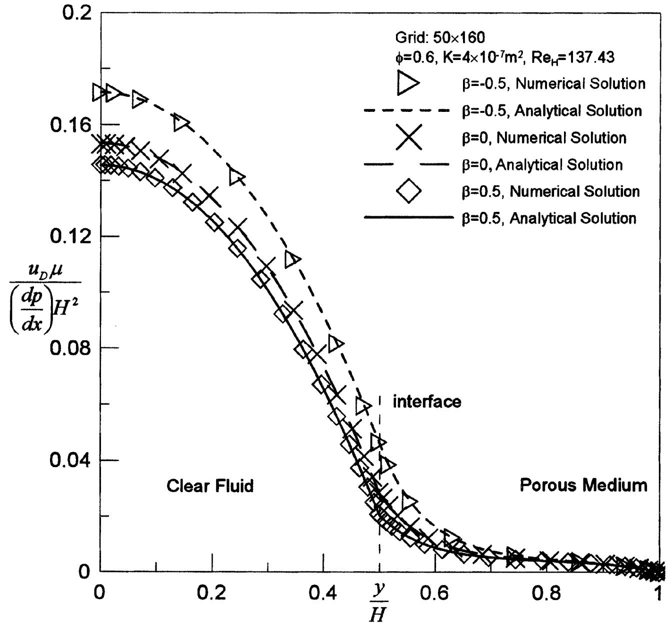

(a)

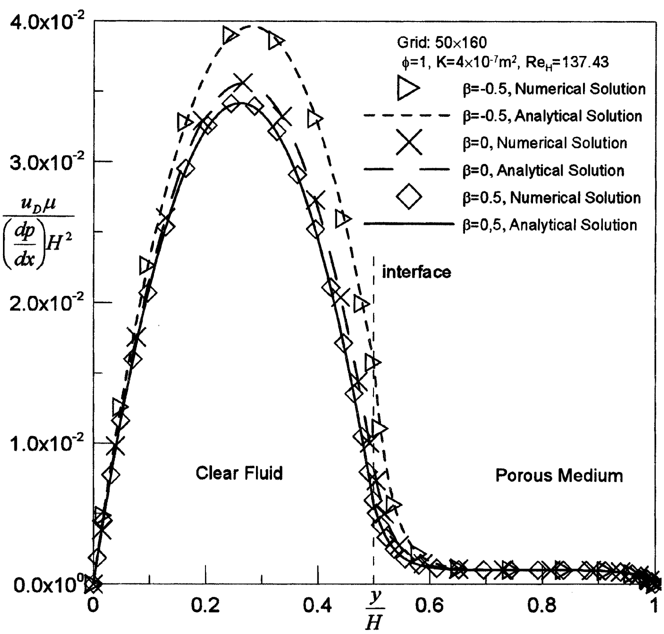

(b)

Figure 6. Comparison between analytical and numerical solution for different values of β: (*a*) without the Fochheimer term; (*b*) with the Forchheimer term.

CONCLUDING REMARKS

Numerical solutions for laminar flow in composite channels were obtained for two situations, namely, considering and neglecting the nonlinear Forchheimer term in the axial momentum equation. Comparison with strictly analytical solution validated the developed numerical tool for situations where the porosity, the permeability, and the jump coefficient were varied. Although results were presented for one-dimensional flows, the implementation herein was done for two-dimensional situations and carried out on a generalized coordinate system. Future applications on complex geometry are expected to contribute to the analysis of important engineering flows.

REFERENCES

1. H. Darcy, *Les Fontaines Publiques de la Vile de Dijon*, Victor Dalmond, Paris, 1856.
2. P. Forchheimer, Wasserbewegung durch Boden, *Z. Ver. Deutsch. Ing.*, vol. 45, pp. 1782–1788, 1901.
3. H. C. Brinkman, A Calculation of the Viscous Force Exerted by a Flowing Fluid on a Dense Swarm of Particles, *Appl. Sci. Res.*, vol. A1, pp. 27–34, 1947.
4. J. Bear, *Dynamics of Fluids in Porous Media*, American Elsevier, New York, 1972.
5. C. T. Hsu and P. Cheng, Thermal Dispersion in a Porous Medium, *Int. J. Heat Mass Transfer*, vol. 33, pp. 1587–1597, 1990.
6. S. Whitaker, Advances in Theory of Fluid Motion in Porous Media, *Ind. Eng. Chem.*, vol. 61, pp. 14–28, 1969.
7. W. G. Gray and P. C. Y. Lee, On the Theorems for Local Volume Averaging of Multiphase System, *Int. J. Multiphase Flow*, vol. 3, pp. 333–340, 1977.
8. J. A. Ochoa-Tapia and S. Whitaker, Momentum Transfer at the Boundary between a Porous Medium and a Homogeneous Fluid—I. Theoretical development, *Int. J. Heat Mass Transfer*, vol. 38, pp. 2635–2646, 1995a.
9. J. A. Ochoa-Tapia and S. Whitaker, Momentum Transfer at the Boundary between a Porous Medium and a Homogeneous Fluid—II. Comparison with Experiment, *Int. J. Heat Mass Transfer*, vol. 38, pp. 2647–2655, 1995b.
10. A. V. Kuznetsov, Analytical Investigation of the Fluid Flow in the Interface Region Between a Porous Medium and a Clear Fluid in Channels Partially Filled with a Porous Medium, *Int. J. Heat Fluid Flow*, vol. 12, pp. 269–272, 1996.
11. A. V. Kuznetsov, Influence of the Stresses Jump Condition at the Porous-Medium/Clear-Fluid Interface on a Flow at a Porous Wall, *Int. Commun. Heat Mass Transfer*, vol. 24, pp. 401–410, 1997.
12. A. V. Kuznetsov, Fluid Mechanics and Heat Transfer in the Interface Region between a Porous Medium and a Fluid Layer: A Boundary Layer Solution, *J. Porous Media*, vol. 2, no. 3, pp. 309–321, 1999.
13. M. J. S. de Lemos and M. H. J. Pedras, Simulation of Turbulent Flow through Hybrid Porous Medium-Clear Fluid Domains, *Proc. IMECE2000—ASME—Int. Mechanical Engineering Congr.*, ASME-HTD-366-5, pp. 113–122, Orlando, FL, November 5–10, 2000.
14. M. H. J. Pedras and M. J. S. de Lemos, Macroscopic Turbulence Modeling for Incompressible Flow through Undeformable Porous Media, *Int. J. Heat Mass Transfer*, vol. 44, no. 6, pp. 1081–1093, 2001.
15. M. H. J. Pedras and M. J. S. de Lemos, Simulation of Turbulent Flow in Porous Media Using a Spatially Periodic Array and a Low Re Two-Equation Closure, *Numer. Heat Transfer A*, vol. 39, no. 1, pp. 35–59, 2001.

16. M. H. J Pedras and M. J. S. de Lemos, On the Mathematical Description and Simulation of Turbulent Flow in a Porous Medium Formed by an Array of Elliptic Rods, *J. Fluids Eng*., vol. 123, no. 4, pp. 941–947, 2001.
17. M. H. J. Pedras and M. J. S. de Lemos, On Volume and Time Averaging of Transport Equations for Turbulent Flow in Porous Media, ASME FED-vol. 248, Paper FEDSM99-7273, 1999.
18. M. H. J. Pedras and M. J. S. de Lemos, On the Definition of Turbulent Kinetic Energy for Flow in Porous Media, *Int. Commun. Heat Mass Transfer*, vol. 27, no. 2, pp. 211–220, 2000.
19. F. D. Rocamora, Jr., and M. J. S. de Lemos, Analysis of Convective Heat Transfer for Turbulent Flow in Saturated Porous Media, *Int. Commun. Heat Mass Transfer*, vol. 27, no. 6, pp. 825–834, 2000.
20. M. J. S. de Lemos and M. H. J. Pedras, Recent Mathematical Models for Turbulent Flow in Saturated Rigid Porous Media, *J. Fluids Eng*., vol. 123, no. 4, pp. 935–940, 2001.
21. F. D. Rocamora, Jr., and M. J. S. de Lemos, Laminar Recirculating Flow and Heat Transfer in Hybrid Porous Medium-Clear Fluid Computational Domains, *Proc. 34th ASME—Natl. Heat Transfer Conf.* (on CD-ROM), ASME-HTD-I463CD, Paper NHTC2000-12317, Pittsburgh, PA, August 20–22, 2000.
22. F. D. Rocamora, Jr., and M. J. S. de Lemos, Heat Transfer in Suddenly Expanded Flow in a Channel with Porous Inserts, *Proc IMECE2000—ASME—Int. Mechanical Engineering Congr*., ASME HTD-366-5, pp. 191–195, Orlando, FL, November 5–10, 2000.
23. R. A. Silva and M. J. S. de Lemos, Flow in a Channel Partially Filled with a Porous Material (in Portuguese), *Proc. 16th Brazilian Congress of Mechanical Engineering* (on CD-ROM), Uberlândia, MG, Brazil, November 26–30, 2001.
24. R. A. Silva and M. J. S. de Lemos, Laminar Flow in a Channel with a Layer of Porous Material Considering the Non-linear Forchheimer Term (in Portuguese), *Proc. II Natl. Cong. Mechanical Engineering* (on CD-ROM), João Pessoa, PB, Brazil, August 12–16, 2002.
25. S. V. Patankar, *Numerical Heat Transfer and Fluid Flow*, Hemisphere, New York, 1980.